NASA/TM-20205000357

Analysis of 100-W Regenerative Fuel Cell Demonstration

William R. Bennett, Phillip J. Smith, and Ian J. Jakupca
Glenn Research Center, Cleveland, Ohio

August 2020

NASA STI Program . . . in Profile

Since its founding, NASA has been dedicated to the advancement of aeronautics and space science. The NASA Scientific and Technical Information (STI) Program plays a key part in helping NASA maintain this important role.

The NASA STI Program operates under the auspices of the Agency Chief Information Officer. It collects, organizes, provides for archiving, and disseminates NASA's STI. The NASA STI Program provides access to the NASA Technical Report Server—Registered (NTRS Reg) and NASA Technical Report Server—Public (NTRS) thus providing one of the largest collections of aeronautical and space science STI in the world. Results are published in both non-NASA channels and by NASA in the NASA STI Report Series, which includes the following report types:

- TECHNICAL PUBLICATION. Reports of completed research or a major significant phase of research that present the results of NASA programs and include extensive data or theoretical analysis. Includes compilations of significant scientific and technical data and information deemed to be of continuing reference value. NASA counter-part of peer-reviewed formal professional papers, but has less stringent limitations on manuscript length and extent of graphic presentations.

- TECHNICAL MEMORANDUM. Scientific and technical findings that are preliminary or of specialized interest, e.g., "quick-release" reports, working papers, and bibliographies that contain minimal annotation. Does not contain extensive analysis.

- CONTRACTOR REPORT. Scientific and technical findings by NASA-sponsored contractors and grantees.

- CONFERENCE PUBLICATION. Collected papers from scientific and technical conferences, symposia, seminars, or other meetings sponsored or co-sponsored by NASA.

- SPECIAL PUBLICATION. Scientific, technical, or historical information from NASA programs, projects, and missions, often concerned with subjects having substantial public interest.

- TECHNICAL TRANSLATION. English-language translations of foreign scientific and technical material pertinent to NASA's mission.

For more information about the NASA STI program, see the following:

- Access the NASA STI program home page at http://www.sti.nasa.gov

- E-mail your question to help@sti.nasa.gov

- Fax your question to the NASA STI Information Desk at 757-864-6500

- Telephone the NASA STI Information Desk at 757-864-9658

- Write to:
  NASA STI Program
  Mail Stop 148
  NASA Langley Research Center
  Hampton, VA 23681-2199

NASA/TM-20205000357

Analysis of 100-W Regenerative Fuel Cell Demonstration

William R. Bennett, Phillip J. Smith, and Ian J. Jakupca
Glenn Research Center, Cleveland, Ohio

National Aeronautics and
Space Administration

Glenn Research Center
Cleveland, Ohio 44135

August 2020

Acknowledgments

The authors would like to thank Bei-Jiann Chang for his experimental design and operation assistance throughout this demonstration.

Level of Review: This material has been technically reviewed by technical management.

Available from

NASA STI Program
Mail Stop 148
NASA Langley Research Center
Hampton, VA 23681-2199

National Technical Information Service
5285 Port Royal Road
Springfield, VA 22161
703-605-6000

This report is available in electronic form at http://www.sti.nasa.gov/ and http://ntrs.nasa.gov/

Analysis of 100-W Regenerative Fuel Cell Demonstration

William R. Bennett, Phillip J. Smith, and Ian J. Jakupca
National Aeronautics and Space Administration
Glenn Research Center
Cleveland, Ohio 44135

Abstract

A 100-W regenerative fuel cell (RFC) demonstration was successfully completed at the NASA Glenn Research Center on December 11, 2014. This effort was funded by Advanced Space Power Systems milestone and represented the first demonstration of passive laboratory-scale stacks arranged as an RFC, consisting of a non-flow-through fuel cell and a static-feed electrolyzer. Once developed, these stacks present the potential to minimize system mass, volume, and parasitic power in comparison to existing terrestrial electrochemical systems and nonnuclear power generation options. Testing involved the fuel cell powering a simulated load then recycling fuel cell product water by subsequently electrolyzing it to regenerate hydrogen and oxygen gases for fuel cell operations. A total of five cycles were completed over a 2-week period, yielding cell voltage data for stack performance and quality measures for regenerated reactants. Overall, round-trip efficiency was calculated to be 47.4 percent. Gas crossover was observed in electrolyzer gas products, as residual gas analysis showed 1.1 percent hydrogen in oxygen and 0.4 percent oxygen in hydrogen. Fuel cell product water was determined to be more acidic and conductive and have a higher fluoride content when compared to deionized water.

Abbreviations

a	chemical activity
CTB	Common Test Bed
DI	deionized, deionizing
E	cell potential
E^0	reversible cell potential
EZ	electrolyzer
F	Faraday constant
FC	fuel cell
ΔG^0	standard state Gibbs free energy
ΔH^0	standard state enthalpy
I	current
MEA	membrane electrode assembly
n	number of moles
NFT	non-flow-through
P	pressure
PEM	proton exchange membrane
PV	photovoltaic
R	ideal gas law constant
RFC	regenerative fuel cell
RGA	residual gas analyzer
SBIR	Small Business Innovation Research

T	temperature
TRL	technology readiness level
V_{th}^{0}	thermoneutral voltage
V_{cell}	single cell voltage

Introduction

Beginning in the 1960s, NASA developed fuel cell technology to power select space missions. The Gemini, Apollo, and Space Shuttle programs all utilized fuel cells of various chemistries to provide auxiliary power. More recently, the NASA Constellation program proposed a proton exchange membrane (PEM) hydrogen regenerative fuel cell (RFC) to power lunar outposts and manned rovers. Evolving fuel cell technology will play a vital role in upcoming lunar missions.

Access to a spaceflight-qualified fuel cell power system ended with the Space Shuttle program. Since the end of the Shuttle program, the greater technology development required by missions to Mars and other extraterrestrial bodies limited interest in and funding for replacing this lost power capability. Thus far, the Space Technology Mission Directorate supported initial hardware development of a passive non-flow-through (NFT) PEM fuel cell technology from a Phase I Small Business Innovation Research (SBIR) contract to technology readiness level (TRL) 4 in laboratory demonstrations (Ref. 1). Operating with pure oxygen, NFT fuel cells separate product water internally by means of a wicking membrane, minimizing parasitic power and system complexity by eliminating the need for oxygen recirculation. The NASA Advanced Exploration Systems Division then funded integrated vehicle public demonstrations in addition to the vacuum and vibration testing necessary to declare the technology a TRL of 5 (Refs. 2 to 4).

A discrete RFC combines a fuel cell with an electrolyzer to produce an energy storage option that is ideally suited for surviving a lunar night. There also exist unitized RFCs in which a single stack performs all electrochemical reactions. Unitized designs present many theoretical advantages, including greater simplicity and lower mass, but significantly lag the technology development of discrete fuel cells and electrolyzers (Refs. 5 and 6).

In an RFC, a power source, such as a photovoltaic (PV) solar array system, provides electricity to the electrolyzer, which produces hydrogen and oxygen gases from water. The PV array is sized to power both the customer load and the electrolyzer while sunlight is available. When sufficient sunlight is no longer obtainable, the hydrogen and oxygen gases are recombined electrochemically within the fuel cell to supply electricity, heat, and water.

It is desirable to consider RFCs when mission energy storage requirements are large enough to make batteries impractical. Over lunar cycle timescales, this generally occurs when system power levels exceed 100s of watts (Ref. 7). While batteries are simpler from a system perspective, passive water management electrochemical stacks serve to reduce RFC system complexity in order to improve reliability and efficiency while reducing overall mass (Refs. 1 and 8).

The purpose of this report is to present voltage data, efficiency calculations, and regenerated reactant quality assessments for the first demonstration of discrete passive fuel cell and electrolyzer stacks employed in an RFC arrangement.

Experimental

The fuel cell and electrolyzer stacks used in this demonstration were prototype research articles on loan from small businesses that are performing SBIR development activities for NASA Glenn Research Center. Both stacks were designed to minimize the requirement for active components, such as pumps and compressors, in order to maximize system reliability and efficiency.

The fuel cell stack, built by Infinity Fuel Cell and Hydrogen, Inc., consisted of seven cells each having an active area of 150 cm^2. This research stack utilized a polymeric water-management membrane with internal provisions to minimize internal resistance and increase efficiency. The mounted fuel cell appears in Figure 1.

The electrolyzer component used for this demonstration was designed and built by Sustainable Innovations, LLC. The electrolyzer stack consisted of five cells, each having an active area of 80 cm^2. The stack was designed for cathode liquid-water feed operation and was equipped with an internal phase separator designed to block the entry of liquid feedwater into the hydrogen gas product. Figure 2 shows the Sustainable electrolysis stack and dedicated test stand.

The RFC system was arranged to collect product water during fuel cell operation in a storage bladder to preclude contact with air. The stored water was transferred to an electrolyzer feedwater tank by gravity through a manual procedure completed when both stacks were offline. Such an arrangement would be conceptually viable in a surface system RFC application. The elevated operating pressure of the fuel cell was used to lift the product water, eliminating the need for a water transfer pump. A mixed-resin deionizing (DI) bed was used to remove water contaminants that could accumulate in and damage the static-feed electrolyzer.

Product water was converted to hydrogen and oxygen during electrolyzer operation with reactants generated at a balanced 200 psia for oxygen and hydrogen. A simplified schematic of the combined RFC elements appears in Figure 3. Opening a manual valve allowed gravity transfer of stored DI product water to the electrolyzer. The electrolyzer product outlets are isolated by operation of solenoid valves and operational pressure was controlled using backpressure regulators. As the stack was a cathode feed design and hydrogen reacts on the cathode side of the electrolyzer membranes, a small cylinder was installed to enable trapping and recirculation of water present in the hydrogen product. Hydrogen and oxygen were locally stored in gas sample cylinders.

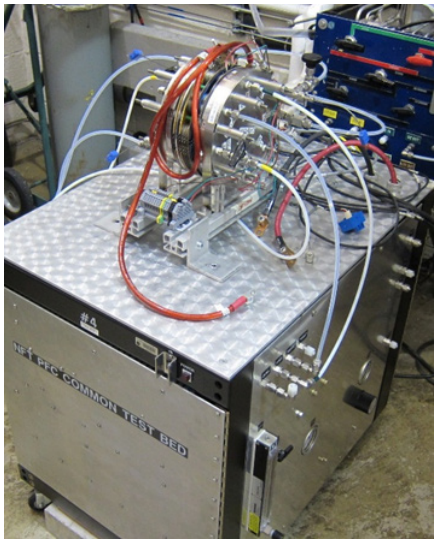

Figure 1.—Fuel cell stack installed on Common Test Bed stand.

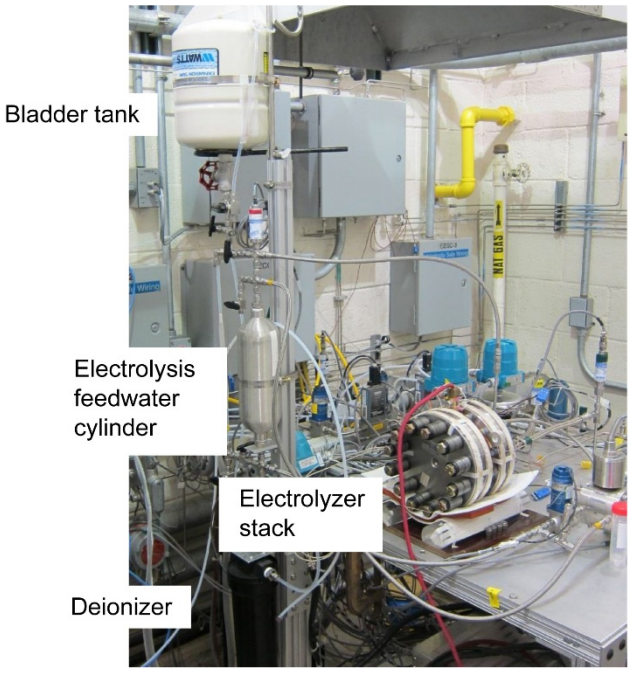

Figure 2.—Electrolysis stack on test stand.

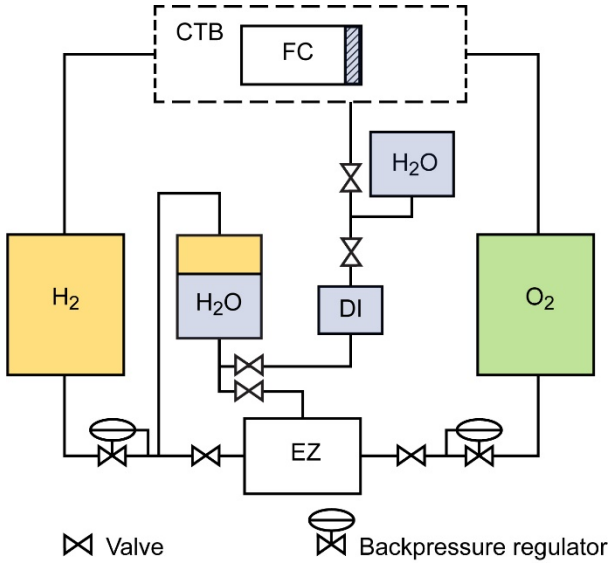

Figure 3.—100-W regenerative fuel cell. Common Test Bed (CTB). Deionizing (DI) column. Electrolyzer (EZ). Fuel cell (FC).

During fuel cell operation, reactant gases flowed from the cylinders to a Common Test Bed (CTB) fuel cell test stand. The CTB contained all required regulators, valves, sensors, and control electronics to operate the NFT fuel cell stack. As the fuel cell generated product water, the CTB collected the water in the previously described bladder accumulator, located above the DI column.

Test Plan

The fuel cell and electrolyzer stacks were operated under vendor-recommended temperature, pressure, and power level conditions. Following preliminary checkout testing, five cycles were completed over a 2-week period. These are denoted as Runs 1 to 5.

The borrowed fuel cell and electrolyzer stacks were not matched in terms of rate capability. The fuel cell consists of seven cells each with 150 cm² active area giving 1,050 cm² of total active area. This is 2.6 times greater than the total active area of the electrolyzer, which comprises five cells each with 80 cm² for an active area totaling 400 cm². Since both stacks operate at a nominal 200 mA/cm² current density, the electrolyzer had to be operated longer than the fuel cell in order to regenerate reactant gas quantities sufficient for fuel cell operation.

Fuel cell testing was conducted at 65 to 70 °C and consisted of steady-state operation at 30 A (200 mA/cm²) and a 2-h standard load profile, which included operation up to 75 A (500 mA/cm²). Cell voltage data provided a measure of efficiency. Hydrogen pressure decay during a rapid shutdown was used to estimate the rate of hydrogen and oxygen recombination in the fuel cell. This data was used to calculate coulombic efficiency.

Electrolysis was performed at 50 °C and consisted of steady-state operation at 16 A (200 mA/cm²) and 24 A (300 mA/cm²). Hydrogen and oxygen production rates were compared with theoretical values to estimate crossover losses and coulombic efficiency. Oxygen pressure was restricted to 200 psia to limit potential for reaction with the titanium structure of the stack. Hydrogen was controlled at 200 psia.

Fuel cell product water and electrolysis gas samples were collected at least once per test run to track the accumulation of contaminants during repeated cycling. To determine the species concentration within the gaseous test samples, the gas was supplied to an Extorr Inc. XT200 residual gas analyzer (RGA). The unit was run in mass spectra collection mode within a high-vacuum system. Once a sample cylinder was connected to this vacuum system, a turbomolecular pump was used to evacuate to approximately 10^{-7} torr, all tubing connecting the cylinder and the RGA. This provided the baseline reading for the analyzer. Sample gas was transferred to the RGA by slightly opening the valve attached to the cylinder and limiting flow with a small orifice needle valve. Once the system pressure stabilized, so that flow from the cylinder to the vacuum pump resulted in a vacuum near 10^{-5} torr, the RGA output data was saved.

Data Analysis

The following Thermodynamic Efficiency and Coulombic Efficiency sections describe how efficiency values were calculated for both the fuel cell and electrolyzer. Data analysis was also necessary to calculate electrolyzer product-gas concentrations from the tabulated RGA data.

Thermodynamic Efficiency

Fuel cell theoretical voltages were computed from tabulated thermodynamic properties, standard Gibbs free energy ΔG^0 and enthalpy ΔH^0, at 65 °C and 1 atm absolute pressure. The reversible cell potential, E^0, is related to the ΔG^0 by Equation (1),

$$\Delta G^0 = -nFE^0 \tag{1}$$

where n is number of moles and F is the Faraday constant.

The thermoneutral voltage V_{th}^0 is related to the ΔH^0 by Equation (2).

$$\Delta H^0 = -nF V_{th}^0 \tag{2}$$

Cell potential E was corrected for pressure using the Nernst equation in Equation (3),

$$E = E^0 - \frac{RT}{nF} \ln \left[\frac{\left(P_{H_2} P_{O_2} \right)^{1/2}}{a_{H_2O}} \right] \tag{3}$$

where R is the ideal gas constant, T is temperature, P_{H_2} is hydrogen pressure in atm, P_{O_2} is oxygen pressure in atm, and a_{H_2O} is the chemical activity of water. The V_{th}^0, a weak function of pressure, was adjusted using an equation of state for oxygen and hydrogen as described in References 9 and 10. For the fuel cell at 65 °C and 44 psia, the theoretical potentials are 1.219 V for E and 1.474 V for V_{th}^0. For the electrolyzer at 50 °C and 200 psia, the theoretical potentials are 1.262 V for E and 1.477 V for V_{th}^0.

Coulombic Efficiency

Assuming the parasitic current, $I_{parasitic}$, representing crossover losses is constant at the stack operational pressure, coulombic efficiency is given by

$$\text{coulombic efficiency} = \frac{I_{actual}}{I_{actual} + I_{parasitic}} \tag{4}$$

where I_{actual} is the measured current output of the stack.

Residual Gas Analyzer

In mass spectra mode, the RGA provides a unitless value for detected intensity of ions across a range of atomic mass units (amu). The amplitude of the reading at various amu allows for determination of relative species concentrations. Within the test samples, only four detectable species were present based on the observed ions and fragment ions: hydrogen at 1, 2, and 3 amu; nitrogen at 14 and 28 amu; oxygen at 16 and 32 amu; and some residual water near 18 amu. The baseline value was subtracted from the test sample amplitude to account for measurement noise and water. To obtain a concentration, the amplitude of all peaks to one species were summed and normalized by the total amplitude of all ions detectable above the baseline value. There is generally a need to account for detection sensitivity when analyzing gases other than nitrogen, however, this method was verified to be accurate to 0.1 mol% using standards of four different known mixtures of hydrogen and oxygen.

Results and Discussion

The results are presented in three major sections: Fuel Cell, Electrolyzer, and Sample Analysis. For both the fuel cell and electrolyzer, polarization curves, thermodynamic efficiencies, and coulombic efficiencies are presented. A round-trip efficiency is provided in the Electrolyzer section. Sample Analysis consists of water pH, fluoride concentration, and conductivity measurements and electrolyzer product gas concentrations.

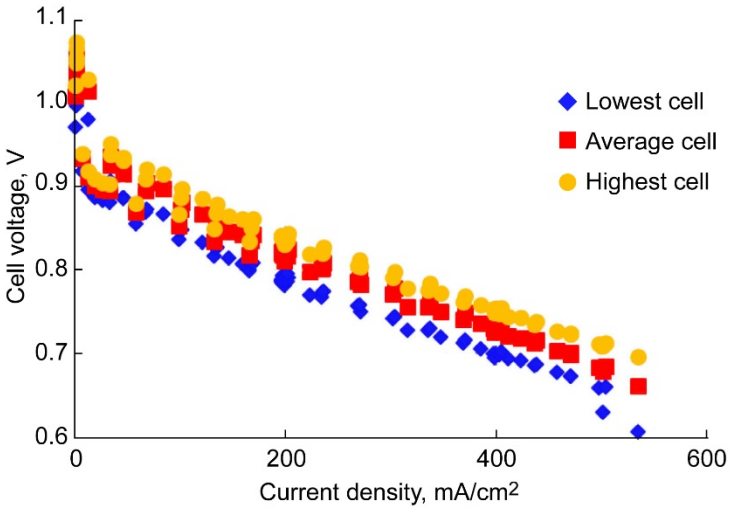

Figure 4.—Fuel cell polarization curve generated at 65 °C.

Fuel Cell

The initial fuel cell polarization curve is presented in Figure 4, providing the lowest, average, and highest cell voltage values collected over a range of current densities throughout testing.

Polarization and variability, or balance, between cells is as expected. Terminal cells, numbers 1 and 7 at the ends of the stack, tend to run at a slightly lower temperature due to contact with the relatively massive 1-in.-thick stainless steel endplates. This likely explains why cell 1 produced the lowest voltage throughout testing. Conversely, cell 4 in the center of the stack was the highest voltage cell over most of the current density range.

Thermodynamic Efficiency

At the nominal operating current density of 200 mA/cm², the resulting average stack performance was 5.74 V and 170 W and the average cell potential was equal to 0.82 V. Relative to the V_{th}^{0}, the equivalent efficiency is calculated to be 56 percent. Therefore, 44 percent of the available energy is lost as heat. This value of efficiency includes heat loss due to the entropy term (Ref. 9).

Relative to the theoretical open-circuit potential of 1.219 V, efficiency is 67 percent. This method for calculating efficiency was used for projected key performance parameter table values, but does not include waste heat due to entropy.

Coulombic Efficiency

Crossover of hydrogen and oxygen across the membrane electrode assembly (MEA) lead to reactant loss during fuel cell operation. The rate of loss can be translated into an equivalent current and used to compute coulombic efficiency. Reactant loss was estimated following an emergency-stop experiment where the stack was isolated from the reactant supply with no applied load. Hydrogen and oxygen pressure decay was observed until equilibration, as presented in Figure 5. This experiment was initiated at 104 min test time during this particular run. Hydrogen pressure decreased more rapidly than oxygen pressure. The hydrogen pressure also reached a minimum at 127 min then started to increase, indicating that it is the limiting reactant and that the hydrogen cavity likely began to fill with oxygen.

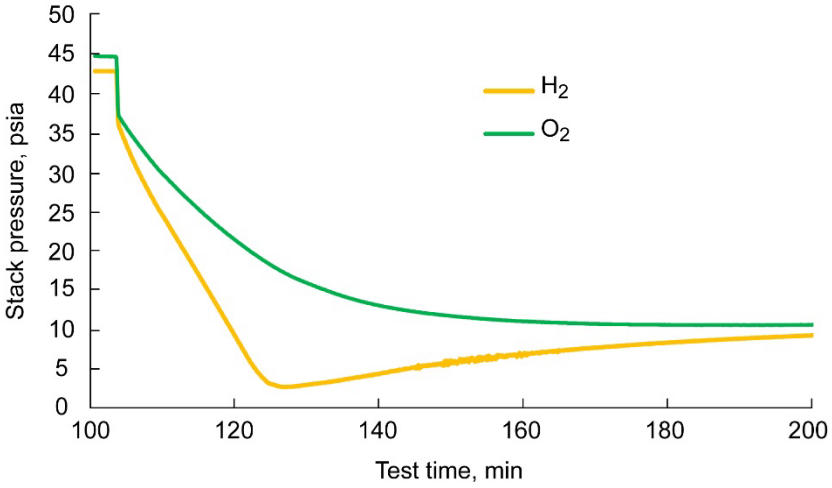

Figure 5.—Fuel cell reactant pressure loss during emergency-stop testing.

TABLE I.—INITIAL DEPRESSURIZATION RATES

Rate	$dP[H_2]/dt$	$dP[O_2]/dt$
psid/min	–2.32	–1.40
atm/s	–.00263	–.00158

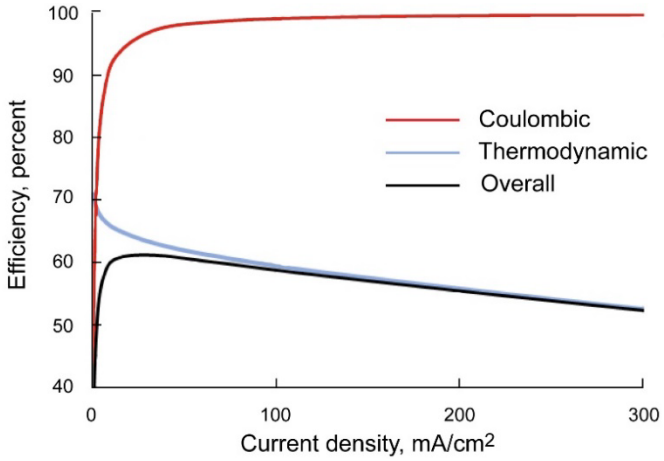

Figure 6.—Projected fuel cell efficiency as function of current density.

Curves were fitted to the initial depressurization data and differentiated to compute the initial rate of decay at 104 min test time. The corresponding decay rates presented in Table I are nearly two to one, as expected from stoichiometry.

Molar rate of hydrogen consumption was estimated using an estimated total internal stack volume, assuming ideal gas behavior. For 55 cm³ of hydrogen at 65 °C, the initial rate of hydrogen consumption is 5.3×10^{-6} mol/s. Assuming this consumption is distributed evenly over the seven cells and applying Faraday's constant, the equivalent parasitic current is 0.1 A or 1 mA/cm^2. At the nominal operating current density, coulombic efficiency is approximately 99.5 percent. The overall efficiency is calculated by multiplying thermodynamic efficiency, 56 percent, and coulombic efficiency giving 55.7 percent for this operating point. For the seven-cell stack tested here, efficiency is strongly dependent on operating current, as shown in Figure 6. Based on these projections, a maximum overall fuel cell efficiency of approximately 62 percent is achieved at 5 A (33 mA/cm^2) with an average cell voltage of 0.93 V.

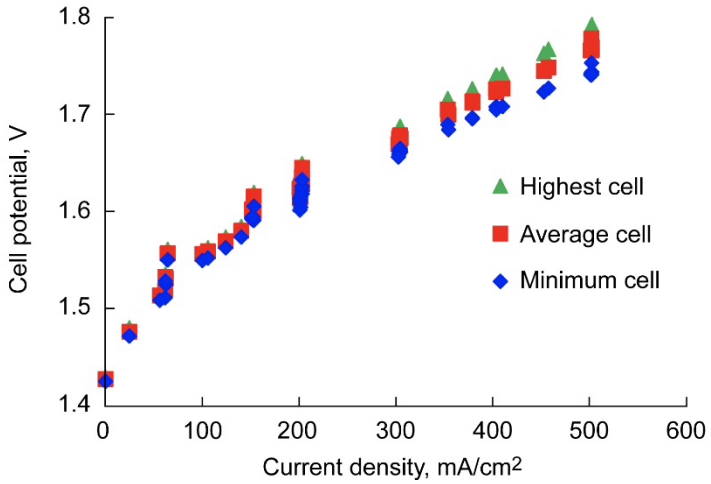

Figure 7.—Electrolyzer polarization data at 50 °C.

TABLE II.—ELECTROLYZER PERFORMANCE AT 200 AND 300 mA/cm²

Current density, mA/cm²	Amps	Volts	Watts	V_{cell}[a] average	Efficiency[b], percent
200	16.3	8.14	132	1.63	90.6
300	24.4	8.38	204	1.68	87.9

[a]Single cell voltage

[b]Efficiency calculated relative to the thermoneutral voltage.

Electrolyzer Results

Polarization performance for the five-cell electrolyzer appears in Figure 7 for the lowest, average, and highest cell voltage values collected over a range of current densities throughout testing. No anomalies were noted in the stack performance.

Thermodynamic Efficiency

At operating current densities of 200 and 300 mA/cm², the electrolyzer stack performance is detailed in Table II.

Coulombic Efficiency

Crossover of hydrogen and oxygen across the MEA lead to reactant recombination in the same manner as in the fuel cell. Coulombic efficiency was estimated by comparing mass flowmeter measured gas flow rate to theoretical values calculated from current. This comparison is shown in Figure 8.

Both oxygen and hydrogen generation rates are slightly below the theoretical line. Fitted slopes are similar, with apparent coulombic efficiency, which is evidenced by gas production, at approximately 94 percent of theoretical. For gas permeation in Nafion™ N117, this result is consistent with literature data, which projects approximately 95 percent coulombic efficiency under these test conditions (Ref. 11).

Round-Trip Efficiency

Based on stack performance measurements, the round-trip efficiency of the 100-W RFC at nominal operating conditions is summarized in Table III. These estimates are for the electrochemical stacks alone and do not include parasitic power from balance-of-plant components. As shown in Figure 6, the overall efficiency of this particular fuel cell stack could reach 62 percent at reduced current density and 0.93 V

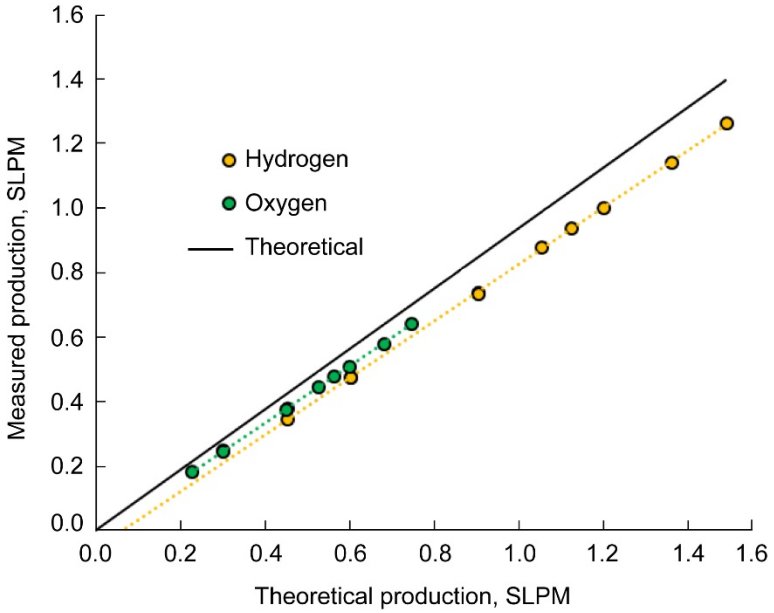

Figure 8.—Electrolysis hydrogen and oxygen production rate.

TABLE III.—REGENERATIVE FUEL CELL (RFC) STACK AND OVERALL EFFICIENCIES

Efficiency, percent	Thermal	Coulombic	Overall
Fuel cell	56.0	99.5	55.7
Electrolyzer	90.6	94.0	85.2
RFC round trip	-------	-------	47.4

cell potential. This change would increase projected round-trip efficiency to 53 percent without changing the hardware design. A real spaceflight system would require significantly more development in regards to the electrolyzer. Storing gases at only 200 psia would be volumetrically prohibitive and crossover issues seem likely when combining high pressures and Nafion™ membranes.

Sample Analysis

Water and gas samples were collected during RFC operations so that product quality could be evaluated. Water samples were tested for pH, fluoride concentration, and ionic conductivity. Results for fuel cell product water and DI electrolyzer feedwater are summarized in Figure 9. Values for freshly dispensed DI water and tap water are included for comparison.

Fuel cell product water showed a slightly acidic pH, between 4.0 and 4.8. This is a typical result based on the 65 °C fuel cell operating temperature (Ref. 12). Fluoride concentration ranged from 0.39 to 1.0 ppm, similar to the tap water sample. Conductivity was between 11 to 43 μS/cm, higher than DI water but much lower than tap water. These results are similar to fuel cell product water samples collected previously from developmental 1- and 3-kW stacks of the same design (Ref. 13). Though some acidity and fluoride is expected from a PEM, due to the gradual release of hydrogen fluoride, the results indicate Nafion™ membrane degradation (Ref. 14). The rate of degradation can be mitigated by operational and material choices.

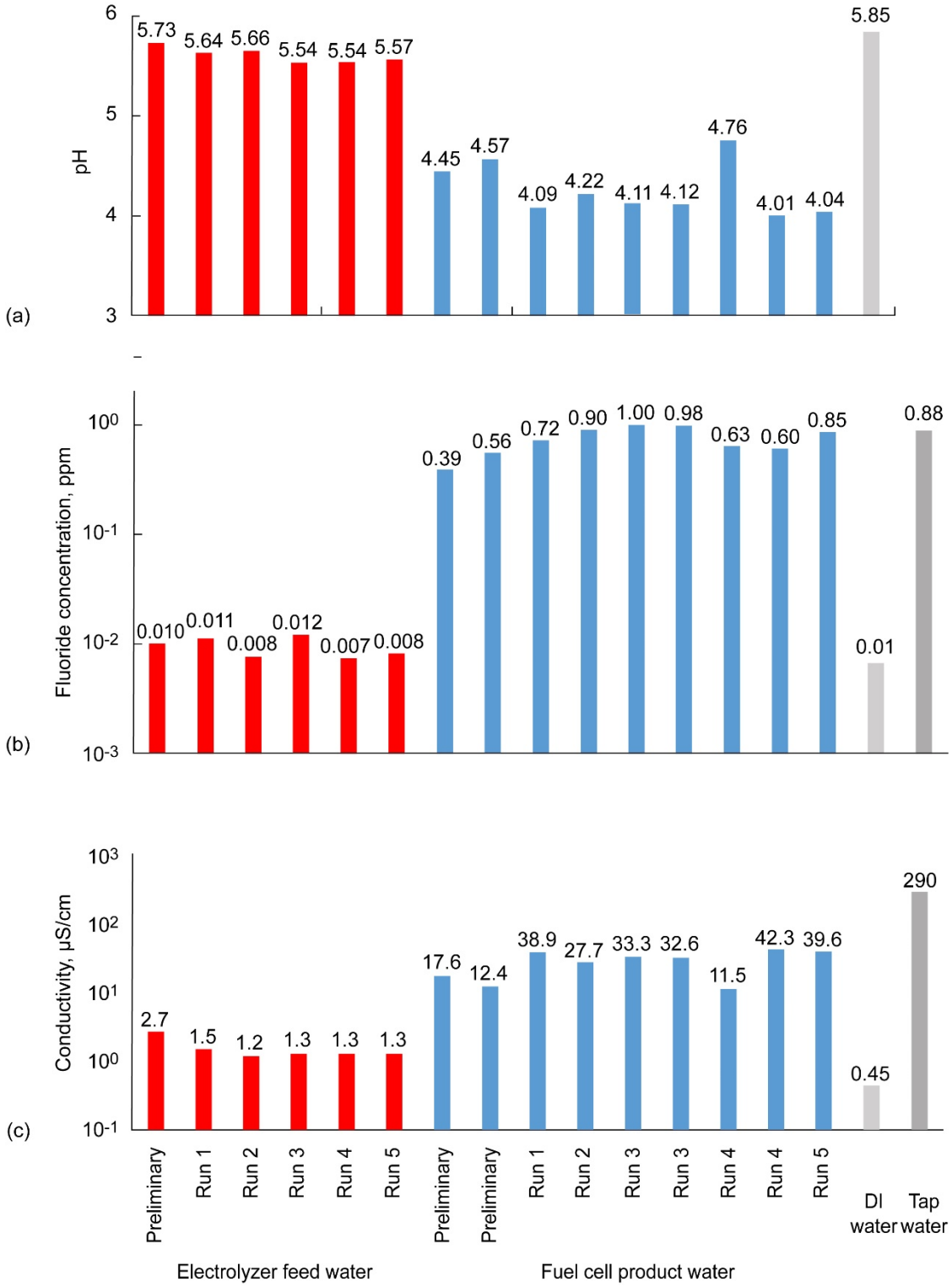

Figure 9.—Water sample analysis for both fuel cell and electrolysis stacks. (a) pH. (b) Fluoride concentration. (c) Conductivity. Deionized (DI).

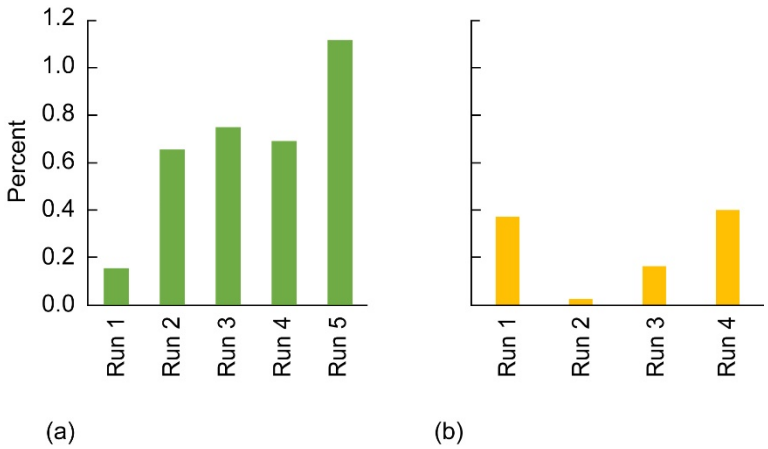

Figure 10.—Electrolyzer product gas analysis. (a) Percent hydrogen in oxygen. (b) Percent oxygen in hydrogen.

Electrolyzer feedwater was most similar to the fresh DI water prepared in the laboratory. This shows the installed DI bed was effective in treating the fuel cell product water prior to transfer to the electrolyzer. The pH ranged from 5.5 to 5.8, only slightly below that of the DI water. The fluoride concentrations and conductivity were both more than an order of magnitude below that of the fuel cell product water.

Residual gas analysis for the five electrolyzer runs is summarized in Figure 10. In the last trial, Run 5, the presence of hydrogen in oxygen was indicated during startup operations by the real-time monitoring sensors, reaching approximately 1.4 percent on that detector. Due to this concern, two gas samples were collected for the oxygen product gas and no sample cylinders were available to collect hydrogen from Run 5. The hydrogen in oxygen concentration was sensitive to changes in hydrogen pressure, likely explaining the higher concentration in the final run. The observed trend of increasing hydrogen in oxygen suggested an internal failure within the electrolysis stack and led to a decision to discontinue testing. The relatively low levels of oxygen in hydrogen may be partly or solely due to air and water contamination of the hydrogen sample during collection and evaluation.

Concluding Remarks

Overall, this first regenerative fuel cell (RFC) demonstration was a successful integration of two passive electrochemical stacks. The five completed cycles provided cell voltage data for stack performance and quality measures for regenerated reactants. Round-trip efficiency was calculated to be 47.4 percent, though that value does not include any balance-of-plant parasitic losses. Gas crossover was observed in the electrolyzer gas products, suggesting a gradual breakdown in the internal integrity of the electrolysis stack. Fuel cell product water was determined to be more acidic and conductive and have higher fluoride content when compared to deionized water.

It appears to be feasible to operate an electrolyzer on fuel cell product water, though that water certainly should be deionized to minimize contamination and corrosion issues. The product water pH could be raised and impurities potentially minimized by reducing fuel cell operating temperature. Future RFC designs and tests should incorporate gas composition analysis to ensure adequate quality and safety in regards to undesirable mixing of hydrogen and oxygen over longer electrolyzer operational periods at elevated hydrogen pressures. While electrochemical stacks were the focus of this project, water management and other balance-of-plant issues will be consequential in further developing integrated RFCs.

References

1. Hoberecht, Mark; Burke, Kenneth; and Jakupca, Ian: The Advantages of Non-Flow-Through Fuel Cell Power Systems for Aerospace Applications. Presented at the Next Generation Suborbital Researchers Conference, Orlando, FL, 2011.
2. Gilligan, Ryan P., et al.: Structural Dynamic Testing Results for Air-Independent Proton Exchange Membrane (PEM) Fuel Cell Technologies for Space Applications. Presented at the ASME International Mechanical Engineering Congress & Exposition, Salt Lake City, UT, 2019.
3. Jakupca, Ian, et al.: Non-Flow-Through Fuel Cell Power Module Demonstration on the SCARAB Rover. AIAA 2017–4611, 2017.
4. Scheidegger, Brianne T.; Burke, Kenneth A.; and Jakupca, Ian J.: Non-Flow-Through Fuel Cell System Test Results and Demonstration on the SCARAB Rover. NASA/TM—2012-217693, 2012. http://ntrs.nasa.gov
5. Moseley, Patrick T.; and Garche, Jurgen, eds.: Electrochemical Energy Storage for Renewable Sources and Grid Balancing. Elsevier, Amsterdam, The Netherlands, 2015.
6. Sadhasivam, Thangarasu, et al.: A Comprehensive Review on Unitized Regenerative Fuel Cells: Crucial Challenges and Developments. Int. J. Hydrog. Energy, vol. 42, no. 7, 2016, pp. 1–19.
7. Guzik, Monica C., et al.: Energy Storage for Lunar Surface Application. AIAA 2018–5106, 2018.
8. Araghi, K.: NASA Non-Flow-Through PEM Fuel Cell System for Aerospace Applications. Presented at IEEE GLOBECOM, Houston, TX, 2011.
9. Onda, K., et al.: Prediction of Production Power for High-Pressure Hydrogen by High-Pressure Water Electrolysis. J. Power Sources, vol. 132, nos. 1–2, 2004, pp. 64–70.
10. LeRoy, Rodney L.; Bowen, Christopher T.; and LeRoy, Donald J.: The Thermodynamics of Aqueous Water Electrolysis. J. Electrochem. Soc., vol. 127, no. 9, 1980, pp. 1954–1962.
11. Barbir, F.: PEM Electrolysis for Production of Hydrogen From Renewable Energy Sources. Sol. Energy, vol. 78, no. 5, 2005, pp. 661–669.
12. Hou, Kung-Hsu, et al.: Analysis of the Characterization of Water Produced From Proton Exchange Membrane Fuel Cell (PEMFC) Under Different Operating Thermal Conditions. Int. J. Hydrog. Energy, vol. 37, no. 4, 2012, pp. 3890–3896.
13. Bennett, William R.; Hoberecht, Mark A.; and Lvovich, Vadim F.: Analysis of Shunt Currents and Associated Corrosion of Bipolar Plates in PEM Fuel Cells. J. Electroanal. Chem., vol. 737, 2015, pp. 162–173.
14. Schlick, Shulamith: The Chemistry of Membranes Used in Fuel Cells. John Wiley & Sons, Inc., New York, NY, 2018.